INT. COMM. HEAT MASS TRANSFER
Vol. 20, pp. 311-322, 1993
Printed in the USA

0735-1933/93 $6.00 + .00

MODELING OF THE GLOBULITIC SOLIDIFICATION OF A BINARY METAL ALLOY

R.J. Feller and C. Beckermann
Department of Mechanical Engineering
The University of Iowa
Iowa City, IA 52242

(Communicated by J.P. Hartnett and W.J. Minkowycz)

ABSTRACT

A model is presented for the globulitic solidification of a binary metal alloy based on the volume averaging and two-phase approaches. The microscopic processes of nucleation and impingement are included in the model, as well as the modeling of species diffusion in the solid and liquid phases while accounting for the movement of the interface. Limiting case results are derived for the Scheil and Lever Rule models, respectively. Simulations are conducted for the Al-4 wt.% Cu system in which the effects of liquid undercooling, cooling rate, impingement, thermophysical properties and spatial effects are studied.

Introduction

Recent work in the area of alloy solidification has centered on the modeling of transport phenomena occurring on macroscopic (system) and microscopic scales as well as the coupling between the two [1-3]. For example, basic nucleation and crystal growth mechanisms at the microscopic scale must be linked with macroscopic heat flow calculations in order to better predict the latent heat evolution and microstructural features on the system scale. In the modeling of equiaxed or globulitic solidification, the usual approach is to consider the species diffusion-limited growth of a single crystal where on a macroscopic scale, species redistribution is neglected [4]. On the other hand, the large value of the Lewis number of metal alloys allows for the assumption of thermal equilibrium to be applied at the microscopic scale and the macroscopic temperature distribution to be obtained from a mixture energy equation.

Recently, the volume averaging process has been applied to the microscopic conservation equations to develop a two-phase model of solidification [5]. The advantage of such a two-phase model is that general macroscopic conservation equations for each phase with corresponding

interfacial balances are derived which directly relate microscopic and macroscopic quantities. The purpose of this study is to apply this model to the globulitic solidification of a binary metal alloy with a simple eutectic-forming phase diagram, i.e., the Al-Cu system. The microscopic processes of nucleation and impingement are included in the model, as well as the modeling of species diffusion in the solid and liquid phases on a microscopic scale while accounting for the movement of the interface. In this fundamental study, simulations are conducted for a simple zero-dimensional system, where certain parametric studies are undertaken, as well as for a one-dimensional system.

Macroscopic Model Equations

The physical system under consideration is shown in Fig. 1, in which a liquid melt of composition C_0 is cooled from one side with the remaining walls considered to be adiabatic and all walls considered to be impermeable. The governing macroscopic equations for no fluid flow are the mixture energy conservation, liquid and solid species conservation and the interfacial species balance equations, obtained by volume averaging the corresponding microscopic equations over an averaging volume, V_0. The averaging volume, shown in Fig. 2, is small compared to the system but large compared to the interfacial structures that develop during the solidification process [5].

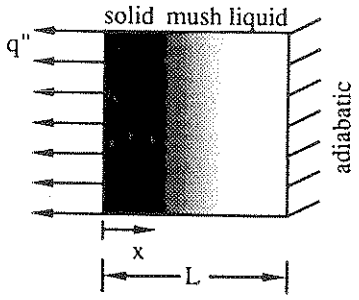

FIG. 1 Schematic of physical system.

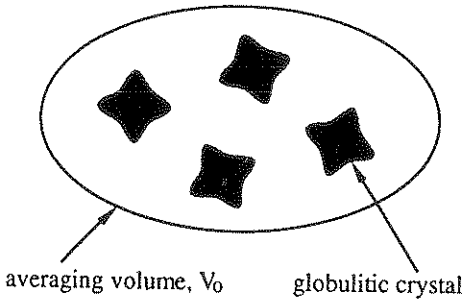

FIG. 2 A typical averaging volume containing globulitic crystals.

The following assumptions apply in the analysis: the crystals grow in the globulitic (spheroidal) morphology; enthalpy is a function of temperature only; thermodynamic equilibrium at the solid/liquid interface with constant liquidus and solidus slopes (κ and m constant); thermal equilibrium between phases within a given averaging volume; identical and constant liquid and solid densities, in which there is no fluid flow in the melt with the solid crystals fixed in space; constant properties, with identical specific heats and thermal conductivities of the liquid and solid phases; no macroscopic species flux. Details of the derivation of the governing macroscopic equations can be found elsewhere [5,6]. They can be written in nondimensional form as

Mixture Energy Conservation

$$\mathrm{Ste}\,\frac{\partial\theta}{\partial\tau} = \mathrm{Ste}\,\frac{\partial^2\theta}{\partial\xi^2} - \frac{\partial\varepsilon_s}{\partial\tau} \tag{1}$$

Liquid Species Conservation

$$(1-\varepsilon_s)\,\frac{\partial\psi_\ell}{\partial\tau} = \frac{1-\varepsilon_s}{1-\kappa}\,\frac{\partial\theta}{\partial\tau} - \left[\Lambda_\ell - \frac{\partial\varepsilon_s}{\partial\tau}\right]\psi_\ell \tag{2}$$

Solid Species Conservation

$$\varepsilon_s\,\frac{\partial\psi_s}{\partial\tau} = \frac{\varepsilon_s\kappa}{1-\kappa}\,\frac{\partial\theta}{\partial\tau} - \left[\Lambda_s D^* + \frac{\partial\varepsilon_s}{\partial\tau}\right]\psi_s \tag{3}$$

Interfacial Species Balance

$$\frac{\partial\varepsilon_s}{\partial\tau} = \frac{1}{\theta+1}\left[\Lambda_\ell\psi_\ell + \Lambda_s D^*\psi_s\right] \tag{4}$$

The dependent variables in eqs. (1) - (4) are the solid volume fraction, ε_s, the dimensionless temperature, θ, and the dimensionless liquid and solid solutal undercoolings, ψ_ℓ and ψ_s, respectively. The Stefan number, Ste, and the mass diffusivity ratio, D*, are defined, respectively, as

$$\mathrm{Ste} = -\frac{\mathrm{cm}C_o}{\Delta h} = \frac{c(T_P - T_L)}{\Delta h} \quad ; \quad D^* = \frac{D_s}{D_\ell} \tag{5}$$

The remaining parameters are defined in the Nomenclature. Additional dimensionless quantities include the interfacial liquid concentration, $\psi_{\ell i}$, and the solutal supersaturation, Ω_k, defined, respectively, as

$$\psi_{\ell i} = \frac{\overline{C}_{\ell i}}{C_o} = \theta + 1 \quad ; \quad \Omega_k = \frac{\overline{C}_{ki} - \langle C_k\rangle^k}{\overline{C}_{\ell i}(1-\kappa)} = \frac{\psi_k}{\psi_{\ell i}} \tag{6}$$

where $\langle C_k\rangle^k$ and $\overline{C}_{ki}$ are the intrinsic volume averaged and average interfacial concentration of phase k, respectively, given as [5]

$$\langle C_k\rangle^k = \frac{1}{V_k}\int_{V_o} X_k C_k\,dV \quad ; \quad \overline{C}_{ki} = \frac{1}{A_i}\int_{A_i} C_k\,dA \tag{7}$$

where X_k is a phase function that is equal to unity in phase k and zero elsewhere. Eqs. (2) - (4) are valid up to the eutectic point, at which point solidification proceeds isothermally such that $\theta = \theta_E$. Then, eq. (1) is used to update the unknown solid volume fraction.

Initial and Boundary Conditions

Initially, the system is entirely liquid and exists isothermally at a given temperature and concentration. Nucleation commences at the nucleation temperature, T_n, which may be below the liquidus temperature. Therefore, the initial ($\tau = 0$) conditions are given as

$$\varepsilon_s = 0 \quad ; \quad \theta = \theta_{in} \tag{8a}$$

$$\psi_\ell = \frac{\theta_n}{1-\kappa} \quad ; \quad \psi_s = \frac{\kappa\theta_n}{1-\kappa} \tag{8b}$$

where θ_n is the dimensionless temperature at nucleation, at which point $\varepsilon_s = \varepsilon_{s,n}$. The boundary conditions for the one-dimensional system are given as

$$\mathrm{Ste}\left.\frac{\partial\theta}{\partial\xi}\right|_0 = -\,Q\xi_L \qquad ; \qquad \left.\frac{\partial\theta}{\partial\xi}\right|_{\xi_L} = 0 \tag{8c}$$

Limiting Cases for a Zero-Dimensional System

A limiting case of the foregoing analysis is that of a zero-dimensional system, in which only one averaging volume is considered. Because no macroscopic spatial variations exist in such a system, the net macroscopic heat flux term appearing in eq. (1) is replaced with a constant volumetric cooling rate, i.e.,

$$\mathrm{Ste}\frac{\partial^2\theta}{\partial\xi^2} = Q \qquad \textit{zero-dimensional system} \tag{9}$$

Eqs. (2) - (4) are identical for zero- and one-dimensional systems due to the assumption of no macroscopic species transport. With such a simplified energy equation, various analytical solutions can be obtained by considering certain limiting cases with regard to species diffusion on a microscopic scale.

The complete mixing of solute in the liquid ($\psi_\ell = 0$) is an important limiting case in practical solidification processes. Further, for the limiting cases of complete and no mixing of solute in the solid it is possible to derive the well-known Lever Rule and Scheil model, respectively [3]. The Lever Rule is derived by summing eqs. (2) and (3) and substituting eq. (4) to eliminate the interfacial terms, setting $\psi_\ell = \psi_S = 0$ and integrating to obtain

$$\psi_{\ell i} = \left[1 - \varepsilon_S(1 - \kappa)\right]^{-1} \qquad \textit{Lever Rule} \tag{10}$$

where θ has been replaced by $\psi_{\ell i}$ according to eq. (6). In a similar manner, the Scheil model is derived by substituting eq. (4) with $D^* = 0$ into eq. (2), setting $\psi_\ell = 0$ and integrating to obtain

$$\psi_{\ell i} = (1 - \varepsilon_S)^{\kappa-1} \qquad \textit{Scheil model} \tag{11}$$

Together with the zero-dimensional energy equation [eqs. (1) and (9)], implicit equations for the solid volume fraction evolution can be derived by differentiating eqs. (10) and (11) with respect to τ, substituting into the energy equation and integrating. The results are

$$Q\tau = \varepsilon_S - \mathrm{Ste}\left\{1 - \left[1 - \varepsilon_S(1 - \kappa)\right]^{-1}\right\} \qquad \textit{Lever Rule} \tag{12}$$

$$Q\tau = \varepsilon_S - \mathrm{Ste}\left[1 - (1 - \varepsilon_S)^{\kappa-1}\right] \qquad \textit{Scheil model} \tag{13}$$

Microscopic Models

The remaining parameters to be specified in eqs. (1) - (4) are the dimensionless interfacial transfer coefficients, Λ_ℓ and Λ_S, which are defined as

$$\Lambda_k = \frac{S_v}{\ell_k n_c^{2/3}} = (48\pi^2)^{\frac{1}{3}} \frac{\varepsilon_s^{\frac{1}{3}} \gamma^{\frac{2}{3}}}{\lambda_k} \delta(\varepsilon_s) \tag{14}$$

Models for the interfacial area concentration, S_v, the diffusion length of phase k, ℓ_k, and the grain density, n, are presented below.

Nucleation

Assuming that nucleation occurs instantaneously at a critical nucleation temperature, T_n, the local and characteristic grain densities, n and n_c, respectively, can be calculated as

$$n = K_1 + K_2 \left(\left. \frac{\partial T}{\partial t} \right|_n \right)^2 \quad ; \quad n_c = K_1 + K_2 \left(\frac{q''}{\rho c L} \right)^2 \tag{15}$$

where the mean cooling rate of the system, - q"/ρcL, has been substituted into the expression for n_c, and K_1 and K_2 are constants determined experimentally for a given alloy [7]. The dimensionless grain density, γ, is then defined as

$$\gamma = \frac{n}{n_c} = K_1^* + K_2^* \left(\left. \frac{\partial \theta}{\partial \tau} \right|_n \right)^2 \tag{16}$$

where K_1^* and K_2^* are dimensionless parameters obtained from the combination of eqs. (15).

Geometric Lengths

Assuming that the volume of a crystal can be characterized by an equivalent spherical volume, the mean solid and final (at $\varepsilon_s = 1$) radius of the crystals, R_s and R_f, respectively, are calculated as

$$R_s = \left[\frac{3\varepsilon_s}{4\pi n} \right]^{\frac{1}{3}} \quad ; \quad R_f = \left[\frac{3}{4\pi n} \right]^{\frac{1}{3}} \tag{17}$$

with the mean liquid radius given as $R_\ell = R_f - R_s$.

Interfacial Area Concentration

During solidification, the interfacial area concentration, $S_v = A_i/V_o$, increases from zero to a maximum value and then decreases again to zero due to the merging of the solid/liquid interfaces and grain impingement. With the assumption of a spherical geometry of crystals, a general expression for S_v can be written as

$$S_v = (36\pi n)^{\frac{1}{3}} \varepsilon_s^{\frac{2}{3}} \delta(\varepsilon_s) \tag{18}$$

where δ is dependent upon the impingement assumption, being equal to unity for no impingement. A general approach has been proposed for the modeling of S_v for impingement under the assumptions that the crystals are fixed in space, impinge randomly and have shape-preserved nucleation and growth transformations subject to subsumed nucleation and growth rate laws [8]. For an approximately constant interfacial velocity and instantaneous nucleation, δ is given as

$$\delta(\varepsilon_s) = \frac{1 - \varepsilon_s}{\varepsilon_s^{\frac{2}{3}}} \left[\ln \frac{1}{1 - \varepsilon_s} \right]^{\frac{2}{3}} \tag{19}$$

Diffusion Lengths

The diffusion length of phase k, ℓ_k, is used to model the microscopic species concentration gradient at the solid/liquid interface. The meanings of the various diffusion lengths are illustrated in Fig. A1. The interface shown represents an infinitesimally small section of the interface of a spherical crystal, and is drawn, for simplicity, as a straight line. ℓ_k is defined as [5]

$$\ell_k = \frac{\overline{C}_{ki} - \langle C_k \rangle^k}{\left. \frac{\partial C_k}{\partial n_k} \right|_i} \tag{20}$$

where $\mathbf{n}_k$ is the outwardly directed unit normal vector on the interface of phase k. After determining the microscopic species profile in each phase, a dimensionless diffusion length, $\lambda_k = \ell_k / R_s$, can be derived for the liquid and solid phases, respectively, as (see Appendix)

$$\lambda_\ell = \frac{1}{Pe\varepsilon_s^{\frac{1}{3}}} \left[1 - \frac{3}{1 - \varepsilon_s} e^{-Pe\varepsilon_s^{\frac{1}{3}}} \int_{\varepsilon_s^{\frac{1}{3}}}^{1} y^2 e^{Pe\varepsilon_s^{\frac{2}{3}} / y} \, dy \right] \quad ; \quad \lambda_s = \frac{1}{5} \tag{21}$$

where y is a dummy variable and Pe is the Peclet number, defined as

$$Pe = \frac{\overline{w} R_f}{D_\ell} = \left(\frac{1}{48\pi^2} \right)^{\frac{1}{3}} \left(\frac{1}{\gamma \varepsilon_s} \right)^{\frac{2}{3}} \frac{\partial \varepsilon_s}{\partial \tau} \tag{22}$$

Numerical Procedure

The separate simulations conducted in zero- and one-dimensional systems required separate numerical procedures to solve the respective system of equations. For the zero-dimensional system, an Adams-Moulton method was used to solve the system of ordinary differential equations, while for the one-dimensional system, the system of partial differential equations was solved using a combined explicit and fully implicit control volume based finite difference scheme

[6]. Time step and grid independence was verified, in which time steps of $\Delta\tau = 10^{-4}$ and 2.5×10^{-4} were used for the zero- and one-dimensional simulations, respectively, with 20 control volumes (Δx = 1.25mm) used for the one-dimensional simulation. Eq. (21) was integrated numerically using a five-point Gaussian rule.

Results and Discussion

The base case parameters for the zero- and one-dimensional simulations are given in Table 1. The thermophysical properties and phase diagram data resemble those of the Al-4 wt.% Cu system ($C_o = 0.04$), in which the properties used (with the exception of D_k) represent averages of liquid and solid quantities between C = 0 and C_E, respectively [9-11]. Here Le = 9620, with K_1^* and K_2^* selected such that the values of K_1 and K_2 in eq. (15) result in a value of n_c consistent with the given quantities of ξ_L and Q with a constraint that $R_f(n) = 1$mm for $\dot{T} = 0$. The zero-dimensional simulation results are presented in Figs. 3, 4 and 5, in which the effects of the mass diffusivity ratio, D^* (with no liquid undercooling), the cooling rate, Q (with no impingement) and the Stefan number, Ste, respectively, are studied. The one-dimensional results are presented in Fig.6. Unless otherwise stated, impingement is assumed in all cases.

TABLE 1. Base Case Parameters [9-11]

Zero-Dimensional System	Common Parameters
$Q = 10$	$\varepsilon_{s,n} = 10^{-9}$
$\theta_{in} = 0$	$\theta_n = 0$
$D^* = 0$	$\theta_E = 7.177$
One-Dimensional System	Ste = 0.04
$Q = 1$	$\kappa = 0.173$
$\xi_L = 0.5$	m = - 373 K/wt.%
$\theta_{in} = -0.1$	$K_1^* = 3.163\times10^{-2}$
$D^* = 10^{-4}$	$K_2^* = 1.550\times10^{-3}$

For the case of no liquid undercooling (Fig. 3), the mass diffusivity ratio D^* is seen to have an influence on ε_s and θ during the later stages of solidification. This is due to the microsegregation occurring in the solid phase, which can clearly be seen in the plot of Ω_s. For intermediate values of D^*, the results are dependent upon the impingement assumption, although the limiting case results given by the Lever Rule and Scheil models, respectively, are independent of this effect as evidenced by eqs. (10) - (13). Note that relatively large (and unrealistic) values of D^* are required to produce discernible differences in ε_s and θ, signifying the relative unimportance of this parameter, although this is not true in the calculation of Ω_s.

A more important parameter governing the solidification process is the cooling rate Q (Fig. 4), which ultimately determines the total solidification time. Note the occurrence of recalescence, i.e., the minimum in the cooling curve brought about by the latent heat release becoming larger than the heat removal, and of the eutectic plateau ($\theta = \theta_E$), where ε_s is a linear function of τ [see mixture energy equation]. Because $D^* = 0$, the Scheil model result is included as a comparison on the plots of ε_s, θ and Ω_s ($\Omega_\ell = 0$ in the Scheil model). The undercooling present in the liquid during the initial solidification stages accounts for the discrepency between the curves, although all cases approach the Scheil limit in the later stages due to the increasingly smaller liquid volumes becoming more well-mixed ($\Omega_\ell \rightarrow 0$). Observable trends for higher cooling rates are the effect of the impingement assumption and the diminishing size of the eutectic plateau.

Fig. 5 shows the effect of another important parameter, Ste, in which again the results in the later solidification stages approach the Scheil limit since $D^* = 0$. Because Ste is dependent upon the initial concentration, C_0, a small value of Ste implies that the melt is of low impurity, which tends to be heat-flow rather than species controlled. In the limit of Ste = 0, ε_s is linear with τ as evidenced by the mixture energy equation. This result is also seen for the Scheil model, eq. (13), as well as the Lever Rule, eq. (12), which reduce to $\varepsilon_s = Q\tau$ for Ste = 0.

Spatial effects can be seen in the one-dimensional results shown in Fig. 6, in which the same general trends in ε_s, θ, Ω_ℓ and Ω_s are seen as in the zero-dimensional case. Note, however, that while recalescence is observed in the first averaging volume, it is not observed for several interior nodes. The recalescence occurring in the deeper interior nodes is due to the reheating effect introduced by the adiabatic boundary condition existing at the right side boundary. This effect is also seen in the plots of Ω_ℓ and Ω_s, although as in the zero-dimensional studies, Ω_ℓ tends to zero as the volumes become fully solid. Fig. 6 also includes the dimensionless final grain radius, $R_f/R_{f,nc} = \gamma^{-1/3}$, which is seen to increase for sequential nodes in the casting (note that $\gamma = 1$ in the zero-dimensional case). This is due to the lower cooling rates experienced away from the cooled boundary, resulting in smaller grain densities and larger grain radii according to eqs. (15) and (17).

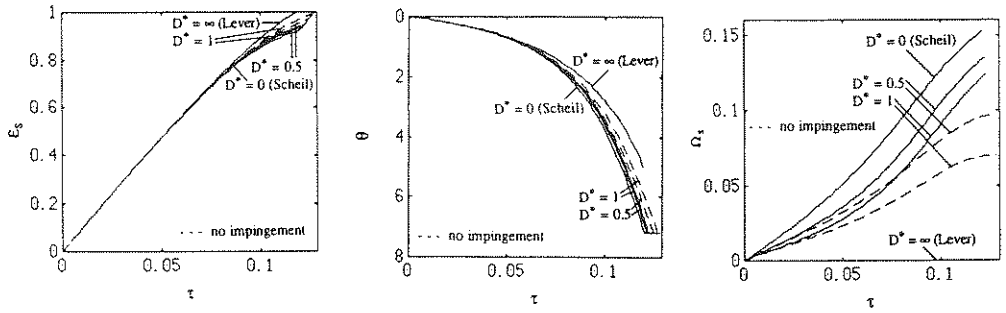

3a) solid volume fraction 3b) dimensionless temperature 3c) solid supersaturation

FIG. 3 Effect of mass diffusivity ratio for no liquid undercooling ($\Omega_\ell = 0$).

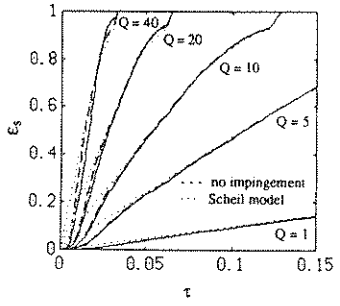

4a) solid volume fraction

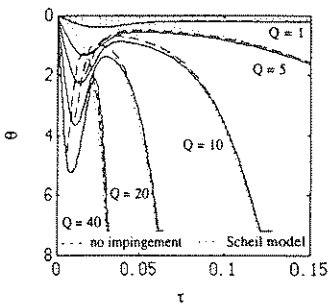

4b) dimensionless temperature

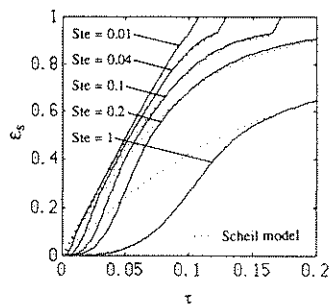

5a) solid volume fraction

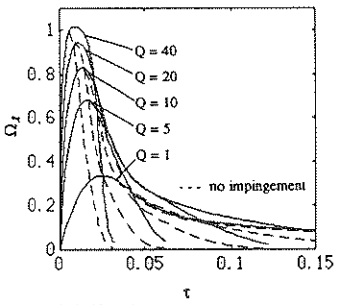

4c) liquid supersaturation

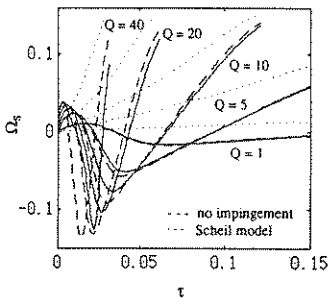

4d) solid supersaturation

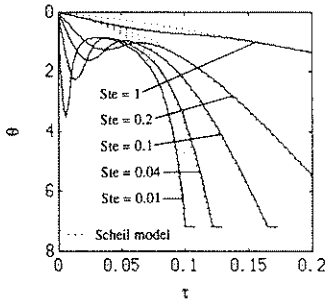

5b) dimensionless temperature

FIG. 4 Effect of cooling rate.

FIG. 5 Effect of Stefan number.

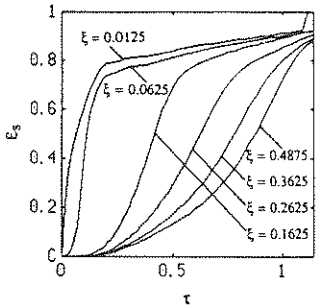

6a) solid volume fraction

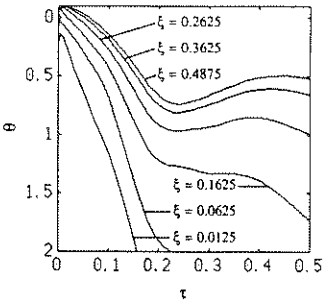

6b) dimensionless temperature

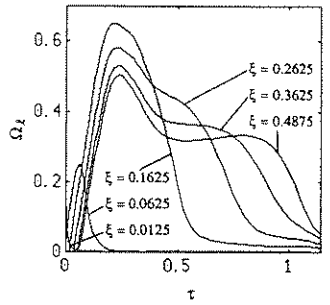

6c) liquid supersaturation

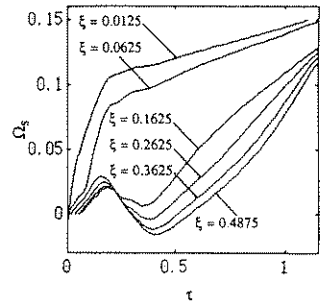

6d) solid supersaturation

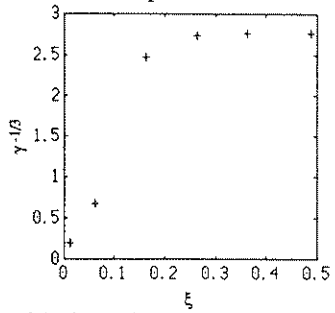

6e) dimensionless final radius

FIG. 6 One-dimensional results.

Conclusions

A micro-macroscopic model was presented for the globulitic solidification of a simple binary alloy in which the microscopic processes of nucleation, impingement and species diffusion were addressed. The microscopic species diffusion process in the liquid was modeled by means of a transformed diffusion equation which accounts for the movement of the growing interface. Limiting case results were derived for the Lever Rule and Scheil models, respectively. Parametric studies were performed in a zero-dimensional system to study various effects such as no liquid undercooling, cooling rate and property ratios. For no liquid undercooling, the effect of the mass diffusivity ratio was seen to be important only in the calculation of the solid supersaturation, in which the effects of microsegregation could be observed. The cooling rate studies showed the importance of the impingement assumption for higher cooling rates, while the Stefan number was shown to represent the degree of impurity in the melt, which greatly influences the solidification process. Subsequent simulations were conducted in a one-dimensional system to represent more practical solidification conditions. Spatial effects were shown in this case, such as the observance of recalescence in different regions of the casting and the distribution of grain sizes. A more complete analysis of this problem, in which the effects of melt convection and solid movement are included, can be found in ref. [12].

Acknowledgments

The authors gratefully acknowledge the support given for this work by the National Science Foundation under Grant No. CBT-8957149.

Nomenclature

a	coefficient in diffusion length model
A	area (m^2)
c	specific heat (J/kg-K)
C	solutal concentration (wt.%)
D	solutal diffusivity (m^2/s)
k	thermal conductivity (W/m-K)
K	coefficient in nucleation model
ℓ	diffusion length (m)
L	length in x direction (m)
Le	Lewis number, α/D_ℓ
m	liquidus slope, $dT/d\overline{C}_{\ell i}$ (K/wt.%)
n	grain density of nuclei (m^{-3})
n	outwardly directed unit normal vector
Pe	Peclet number, $\overline{w}R_f/D_\ell$
q"	wall cooling flux (W/m^2)
Q	dimensionless cooling rate, $q''/\rho\Delta h D_\ell n_c^{2/3} L$
r	radial coordinate
R	radius (m)
Ste	Stefan number, $-cmC_o/\Delta h$
S_v	interfacial area concentration, A_i/V_o (m^{-1})
t	time (s)
T	temperature (K)
V	volume (m^3)
w	interfacial velocity, dR_s/dt (m/s)
x	spatial coordinate (m)
X	phase function
z	moving coordinate (m)
Δh	latent heat of fusion (J/kg)

Greek Symbols

α	thermal diffusivity (m^2/s)
δ	interfacial area concentration parameter
ε_k	volume fraction, V_k/V_o
γ	dimensionless grain density, n/n_c
κ	segregation coefficient, $\overline{C}_{si}/\overline{C}_{\ell i}$
λ_k	dimensionless diffusion length, ℓ_k/R_s
Λ_k	dimensionless interfacial transfer coefficient, $S_v/\ell_k n_c^{2/3}$
ρ	mass density (kg/m^3)
θ	dimensionless temperature, $(T - T_L)/mC_o$
τ	dimensionless time, $tD_\ell n_c^{2/3}$
ξ	dimensionless x distance, $xn_c^{1/3}/\sqrt{Le}$
Ω_k	solutal supersaturation, $(\overline{C}_{ki} - \langle C_k \rangle^k)/\overline{C}_{\ell i}(1 - \kappa)$
ψ_k	dimensionless solutal undercooling, $(\overline{C}_{ki} - \langle C_k \rangle^k)/C_o(1 - \kappa)$
$\psi_{\ell i}$	dimensionless interfacial liquid concentration, $\overline{C}_{\ell i}/C_o$

Subscripts

c	characteristic
E	eutectic
f	final
i	interfacial
in	initial
k	phase k
ℓ	liquid
L	liquidus corresponding to C_o
n	nucleation
o	averaging
P	pure substance
s	solid

Superscripts

$\overline{\ }$	interfacial average, mean
*	dimensionless property
$\cdot$	time-dependent rate

References

1. M. Rappaz and D.M. Stefanescu, in *Solidification Processing of Eutectic Alloys* (Edited by D.M. Stefanescu, G.J. Abbaschian and R.J. Bayuzick), p. 133, The Metallurgical Society (1988).
2. M. Rappaz, Int. Mat. Rev. *34*, No. 3, p. 93 (1989).
3. W. Kurz and D.J. Fisher, *Fundamentals of Solidification*, 3rd ed., Trans Tech, Aedermannsdorf, Switzerland (1989).
4. M. Rappaz and Ph. Thevoz, in *Materials Processing in the Computer Age* (Edited by V.R. Voller, M.S. Stachowicz and B.G. Thomas), p. 321, The Minerals, Metals & Materials Society (1991).
5. J. Ni and C. Beckermann, Metall. Trans. *22B*, p. 349 (1991).
6. R.J. Feller, *M.S.M.E. Thesis*, The University of Iowa, Iowa City, Iowa (1991).
7. D.M. Stefanescu, G. Upadhya and D. Bandyopadhyay, Metall. Trans. *21A*, p. 997 (1990).
8. R.A. Vandermeer, R.A. Masumura and B.B. Rath, Acta Metall. Mater. *39*, No. 3, p. 383 (1991).
9. L.F. Mondolfo, *Aluminum Alloys - Structure and Properties*, Butterworth, London (1976).
10. T.P. Battle and R.D. Pehlke, Metall. Trans. *21B*, p. 357 (1990).
11. J.L. Murray, Inter. Met. Rev. *30*, p. 211 (1985).
12. C. Beckermann and J. Ni, Journal of Materials Processing and Manufacturing Science (in press, 1993).

Appendix

The diffusion length in the liquid region, ℓ_ℓ, is derived by transforming the stationary unsteady one-dimensional spherical diffusion equation into that of a coordinate system which moves with the interface as shown in Fig. A2. For constant $\overline{w}$, the moving coordinate, z, is

defined as

$$z = \left[r^3 - R_S^3\right]^{\frac{1}{3}} \tag{A1}$$

By introducing eq. (A1) into the diffusion equation, applying the chain rule of differentiation and converting back to stationary coordinates, the diffusion equation for quasi-stationary conditions ($dC_\ell/dt = 0$) and its general solution are given as

$$\frac{d^2C_\ell}{dr^2} + \left[\frac{2}{r} + \frac{\overline{w}}{D_\ell}\frac{R_S^2}{r^2}\right]\frac{dC_\ell}{dr} = 0 \qquad ; \qquad C_\ell(r) = a_1 + a_2\, e^{\overline{w}R_S^2/D_\ell r} \tag{A2}$$

The constants, a_i, are determined by application of the following conditions:

$$C_\ell(R_S) = \overline{C}_{\ell i} \qquad ; \qquad \langle C_\ell \rangle^\ell = \frac{3}{(R_f^3 - R_S^3)}\int_{R_S}^{R_f} C_\ell(r)\, r^2\, dr \tag{A3}$$

ℓ_ℓ is then calculated from eq. (20), with the result given as

$$\ell_\ell = \frac{D_\ell}{\overline{w}}\left[1 - \frac{3}{(R_f^3 - R_S^3)}\, e^{-\overline{w}R_S/D_\ell}\int_{R_S}^{R_f} r^2\, e^{\overline{w}R_S^2/D_\ell r}\, dr\right] \tag{A4}$$

In the derivation of the solid diffusion length, ℓ_S, a quadratic distribution is assumed for $C_S(r)$, in which the unknown coefficients are determined by application of the interfacial and symmetry conditions as well as the equation for $\langle C_S \rangle^S$, calculated from eq. (7). ℓ_S is then calculated from eq. (20), given as

$$\ell_S = \frac{1}{5} R_S \tag{A5}$$

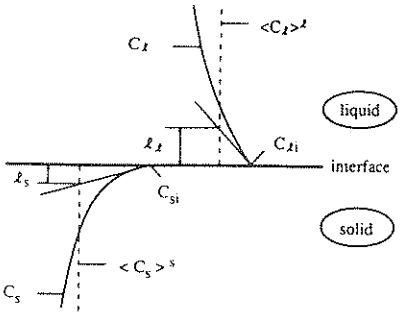

FIG. A1 Schematic illustration of the diffusion lengths [5].

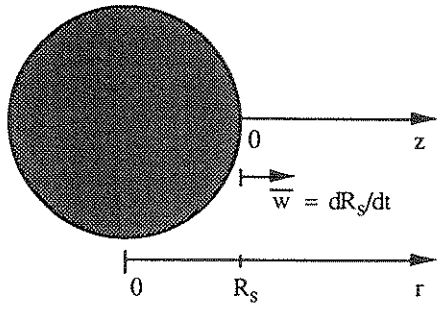

FIG. A2 Schematic of moving coordinate system in the liquid region.

Received December 15, 1992